

GRAIN SIZE ESTIMATION IN STEELS

ANTONÍN ŠEVČÍK¹, KATARÍNA ŠULLEIOVÁ¹, MICHAL BESTERCI¹,
IVAN KOHÚTEK¹, IVAN SAXL^{2*}

Metallographic analysis of the primary austenitic grain of carbon steels after various thermal treatment is carried out. Two methods are examined in detail: the ASTM recommended procedure and the recently proposed method based on stochastic simulations of convex space filling systems. The difference between the profile size and 3D grain size estimates based on the profile and intercept counts occurring in heterogenous grain structures and to certain degree also in structures with mild size dispersion is removed in the latter case. An attention is given also to the possibilities to separate the components of the heterogeneous grain structures.

Key words: carbon steels, duplex grain structures, grain size estimation, primary austenitic grain, w - s diagram

ODHAD VELIKOSTI ZRNA V OCELÍCH

V práci je provedena metalografická analýza primárního austenitického zrna uhlíkových ocelí po různých tepelných zpracováních. Detailně jsou zkoumány dvě metody: postup doporučený ASTM a současně navržená metoda založená na stochastických simulacích konvexních systémů zcela vyplňujících prostor. Rozdíl v odhadech velikosti profilu a trojrozměrných zrn založených na počítání profilů a průsečíků, objevující se u heterogenních struktur a v jisté míře i u struktur s malou disperzí rozměrů, je odstraněn při použití druhého postupu. Pozornost je také věnována možnostem separace složek heterogenní struktury zrn.

1. Introduction

A complicated situation frequently encountered in metallography are grain structures formed by two fractions of grains more or less differing in the size characteristics. A more detailed classification of the grain size is then necessary for a correct interpretation of mechanical properties as the barrier effect of high angle boundaries in blocking the movement of slip dislocations as well as the propagation

¹ Institute of Materials Research, Slovak Academy of Sciences, Watsonova 47, 043 53 Košice, Slovak Republic

² Mathematical Institute, Academy of Sciences of the Czech Republic, Žitná 25, 115 67 Praha 1, Czech Republic

* corresponding author, e-mail: saxl@math.cas.cz

of a cleavage fracture can be quite incorrectly assessed if it is based on the mean grain size of such a two-component structure.

However, the grains cut by the planar or line section are not sampled by their number but by their properties, namely large grains are cut more frequently than the small ones and, consequently, the coarser fraction is more numerous in induced tessellations than in the original 3D one. Moreover, a separation of profiles by their size is difficult as an appreciable number of small profiles and chords is produced by grains of an arbitrary size, in particular, if they are of polyhedral shape. Fortunately, the grains and profiles of individual fractions are frequently not completely intermixed and form continuous regions filled by sections of grains of the same type.

Recently, a method of grain size estimation (including also the estimate of the mean grain volume $\mathbf{E}v$ or, equivalently, of the spatial grain intensity $N_V = 1/\mathbf{E}v$) was proposed [1]. It is based on the simultaneous estimation of the mean profile area $\mathbf{E}a$, mean intercept length $\mathbf{E}l$ and coefficients of variation $CV a$, $CV l$. The starting point of the analysis are the approaches recommended by the ASTM E 112 Standard methods for determining average grain size. However, this method – because of its generality – cannot assure a comparable accuracy for a wide range of materials occurring in practice. Additional corrections taking into account particular features of the examined grain structure are then necessary or at least recommendable. The important tool of the improved analysis is the w - s diagram which records in an illustrative manner the mutual relation between the basic grain characteristics: the average mean breadth (the mean Feret diameter) $\mathbf{E}w$ and the mean surface $\mathbf{E}s$. The counterpart of this 3D relation is the connection between the mean profile area and the mean intercept length. The diagram is based on the extensive database of random 3D Voronoi tessellations [2], which are suitable stochastic models of polyhedral grain structures. The manual and automatic image analysis of simulated planar sections described in [3] demonstrate all advantages and pitfalls of the method. Its application to a fairly homogeneous real grain structure of a Cu-based system is described in [4].

In the present paper, several less or more polydispersed (heterogeneous) primary austenitic grain structures of low alloyed steels after various thermal treatments are examined. It should be underlined that just the grain structures of these specimens initiated the research two years ago and, in particular, inspired the development of the Bernoulli cluster field and tessellations generated by it [1, 5]. They cover a wide range of model unimodal and multimodal tessellations with practically unlimited size dispersion.

2. Material

Distinctly heterogeneous grain is commonly observed in carbon steels stabilized by Al; various grain structures are formed depending on the temperature and

annealing time in the range of the austenitic grain growth. This effect has been observed in fine-grained low carbon steels [6] and is sometimes believed to represent the secondary recrystallization. Similar situation occurs also in carbon steels possessing ferritic-perlitic structure and its proper evaluation is necessary for the interpretation of their strength, plasticity and brittleness.

The examined specimens are carbon steels obtained by diverse thermal treatment of 18 specimens from 16 batches; the range of their chemical composition is shown in Table 1 [7, 8]. The analysed primary austenitic grain was revealed by etchants based on the picric acid.

Table 1. Chemical composition of examined carbon steels

Element	C	Mn	Si	S	P	O	N
Weight %	0.4-0.6	0.6-0.9	0.1-0.4	0.03-0.06	0.01-0.03	0.003-0.009	0.003-0.009

Three characteristic grain structures were observed depending on the temperature of the thermal treatment [9]:

1. Fine and visually only mildly inhomogeneous austenitic grain of the size $G \approx 8$ ($N_A \approx 2000 \text{ mm}^{-2}$) developed at temperatures below 1000°C – Fig. 1 (specimens M).

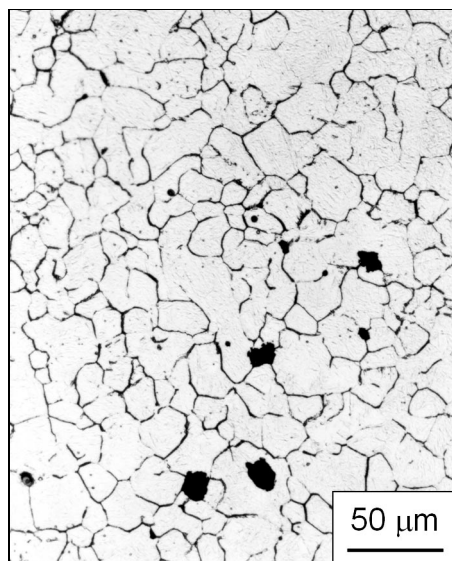


Fig. 1. Specimen M3, $950^\circ\text{C}/90 \text{ min.}$

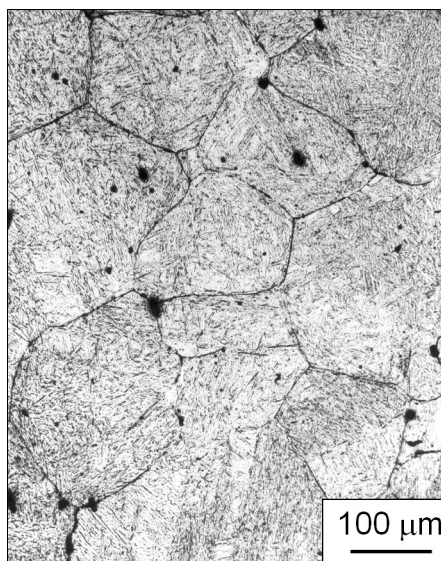


Fig. 2. Specimen V3, $1100^\circ\text{C}/180 \text{ min.}$

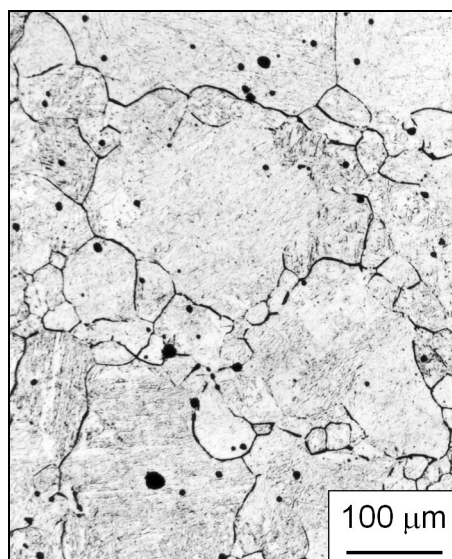


Fig. 3. Specimen S3, 1000 °C/90 min.

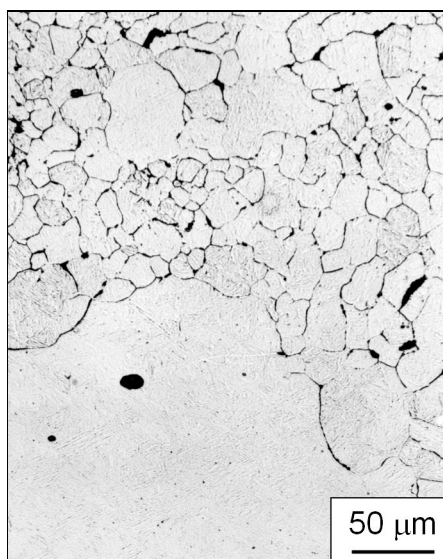


Fig. 4. Specimen S7, 980 °C/45 min.

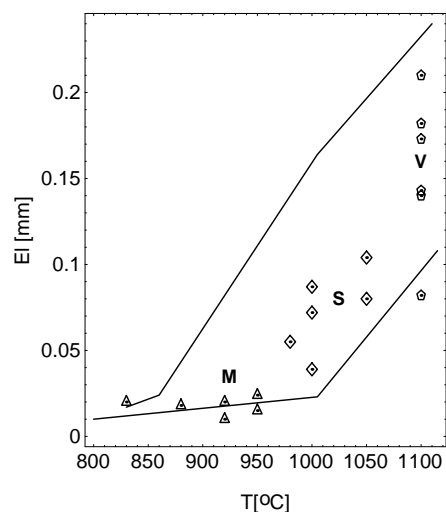


Fig. 5. The effect of the thermal treatment temperature on the mean intercept lengths El of the examined specimens M, S, V (points) and the expected range of El proposed in [10] (lines).

2. The homogeneous austenitic grain of larger size $1 < G < 3$ ($16 < N_A < 64$ [mm^{-2}]) was formed at the temperature 1100 °C; the profile homogeneity or uniformity was roughly the same as in the previous case – Fig. 2 (specimens V).

3. The heterogenous grain structure consisting of very large grains surrounded by regions of considerably finer grains developed in the medium temperature range. The size of the large grains was occasionally considerably greater than in the high temperature range – Figs. 3, 4 (specimens S). Such an exaggerated grain growth has been observed only in some specimens whereas other specimens of the same batch and thermal treatment and sampled in similar locations exhibited a normal behaviour.

The above described behaviour of examined steels on annealing demonstrates Fig. 5, in which selected results are presented of the intercept length measurements. The grain structure formed by a decomposition of the heterogeneous austenite grain consists of regions formed by perlitic grains of two distinctly different sizes. In the fine grain regions – perhaps as a consequence of a local destabilization of austenite – also an increased amount of proeutectoid ferrite can be observed.

3. Methods of estimation and results

The ASTM E 112-82 approach is discussed at length in Vander Voort [11] and recently in [12]. In order to obtain the same estimate of the ASTM grain size number G by the profile count as well as by the intercept count, the factor $[c]_{N_L, N_A} = [N_A]/([N_L]^2)$ must be constant; the brackets $[\]$ denote estimators and their superscript the quantities involved in the estimate, namely the areal density of profiles N_A and the line density of intercepts N_L . The knowledge of other two factors c', c'' makes also estimating of the spatial density N_V possible: $N_V = c' N_A^{3/2}$, $N_V = c'' N_L^3$. The relations of $\mathbf{E}w = (c')^{-2/3}$, $\mathbf{E}s = 4(c'')^{-1/3}$ hold for $N_V = 1$, where $\mathbf{E}w, \mathbf{E}s$ are the mean grain breadth and the mean grain surface (for details see [1, 3, 12]). $\mathbf{E}w, \mathbf{E}s$ are independent quantities with the lower bound 0 and, consequently, the factors c, c', c'' can be considered as at least approximately constant only for grain structures one way or another similar. The mutual relation of the factors $c = (c''/c')^{2/3}$ is not dependent on the actual grain size. The values of the factors proposed in the ASTM, Czech and Slovak Standards are shown in Table 2 together with the corresponding values of $\mathbf{E}w, \mathbf{E}s$ for a unit (i.e. $N_V = 1/\mathbf{E}v = 1$) 3D grain structure and of the mean intercept length $\mathbf{E}l = 1/N_L$ in a planar unit sectional (induced) tessellation $\mathbf{E}a = 1/N_A = 1$. It must be stressed that in contrast to the factor c , the factors c', c'' cannot be directly estimated from plane and line sections.

Specimen notation, their thermal treatment, magnifications of analysed photomicrographs, examined areas, and the main results are summarized in Table 3.

Profile and chord characteristics. The profile densities N_A have been simultaneously determined by manual and automatic image analysis (AIA, the DIPS 5.0

Table 2. Values of factors c, c', c'' postulated in Czech, Slovak and US standards and the corresponding values of $\mathbf{E}v'', \mathbf{E}w, \mathbf{E}s$

Standard	c	c'	c''	$\mathbf{E}l$ [$N_A = 1$]	$\mathbf{E}w$ [$N_V = 1$]	$\mathbf{E}s$ [$N_V = 1$]
ASTM	0.794	0.8	0.566	0.891	1.16	4.84
	0.785	0.813		0.886	1.148	
CZ, SK	0.788	1	0.7	0.887	1	4.505

The first line corresponds to the formally postulated value $1/c = 1.26$.

Table 3. Effect of thermal treatment on the estimated characteristics, ASTM grain size numbers

Spec. No.	TT [°C/min]	M	Area [mm ²]	N_A [mm ⁻²]	N_L [mm ⁻¹]	$G(a)$	$\Delta G/G$ [%]	$CV a$	$CV l$	c
M1	830/90	500	0.08	2113	50.3	8.09	1.0	0.97	0.64	0.84
M5	880/180	250	0.26	1647	42.55	7.73	2.55	0.90	0.64	0.91
M4	920/90	250	0.265	7771	100.0	9.96	-0.44	1.20	0.65	0.77
M2	920/180	320	0.174	2313	50.3	8.22	2.40	1.40	0.71	0.91
M3	950/90	250	0.311	2558	58.4	8.37	1.38	1.00	0.71	0.86
M6		200	0.48	2870	68.5	8.53	-4.45	1.00	0.57	0.61
S7	980/45	200	≈ 0.53	≈ 600	≈ 18	≈ 4.2	≈ 29	-	-	-
S1	1000/22.5	150	0.78	681	25.9	6.1	5.9	1.05	0.75	1.02
S4	1000/45	125	1.05	260	13.9	5.07	15.1	2.95	0.94	1.35
S3	1000/90	125	1.09	152	11.5	4.29	12.5	2.82	1.13	1.15
S6	1050/22.5	100	1.77	166	12.5	4.42	9.45	2.60	0.96	1.06
S5	1050/45	100	2.1	153	9.6	4.30	24.8	3.05	1.03	1.66
V1	1100/22.5	200	0.428	62	8.45	3	3.86	1.20	0.82	0.86
V2		160	0.768	141	14.5	4.19	-5.83	1.21	0.71	0.67
V5	1100/45	100	2.01	47	7.72	2.60	-0.2	1.17	0.61	0.79
V6		100	1.83	28	5.98	1.85	-1.35	0.90	0.53	0.78
V4	1100/90	100	1.72	29	5.87	1.90	4.31	1.00	0.71	0.84
V3	1100/180	100	1.85	22	5.39	1.51	-4.14	0.76	0.59	0.76

analyser) and the proper edge corrections have been made; the areas a_i of individual profiles have also been estimated in the latter case. The results of AIA have been typically higher (by 10%, say). The reason of this discrepancy is that AIA considers as profiles also small inclusions or other imperfections on the micrograph. Only if the number of profiles is small (V specimens), a complete agreement between manual analysis and AIA can be attained. Also the effect of a finite thickness of the grain boundary traces was not negligible and the total profile area was only kW , $0.9 \leq k \leq 0.95$, where W is the observing window area. Consequently, only the results of the manual analysis have been used to calculate N_A whereas profile areas a_i served only to the estimation of the coefficient of variation $CV a$. In order to include also the profiles intersecting the boundary of the observing window, the areas a'_i of incomplete profiles have been randomly paired and $CV a$ estimated as the mean value corresponding to 10 such random pairings (Table 3).

Chords have been not only counted but also measured and $El = 1/N_L$ as well as the coefficient of variation $CV l$ have been directly estimated. The edge effects have been excluded by the same manner as in the case of profile areas, namely the test lines crossing the whole observing window have been used and the segments

at the ends of test lines have been randomly paired. The factor c was estimated by the above given estimator $[c]_{N_L, N_A}$.

Mean values of selected quantities together with the total numbers of observed (counted) profiles $n(a)$ and intercept lengths $n(l)$ and coefficients of error of the means (relative standard deviation of the sample mean) CE $\mathbf{E}a$, CE $\mathbf{E}l$ for specimens of the types M, S, V are summarized in Table 4.

Table 4. Selected mean values

	$n(a)$	$n(l)$	CE $\mathbf{E}a$ [%]	CE $\mathbf{E}l$ [%]	c	CV a	CV l	G	$ \Delta G $
M	200–2000	50–150	3–7	5–9	0.81	1.05	0.65	8.5	0.16
S)*	200–500	60–100	17–22	17–23	1.25	2.5	0.96	4.8	0.63
V	25–100	30–60	12–23	8–16	0.78	1.04	0.66	2.5	0.09

)* specimen S7 not included

Grain size estimation. The ASTM grain size number is defined by $G(a) = -2.9542 + 3.3219 \log N_A$ (CZ and SK Standards set $g(a) = -3 + 3.3219 \log N_A$, from which the difference $G - g = 0.0458$ follows).

For the intercept (Heyn) method, the recommended formula $G(l) = 6.6439 \log N_L - 3.2877$ has been used to estimate the ASTM grain size number (CZ and SK Standards set $g(l) = 6.6439 \log N_L - 3.34275$; then $G(l) - g(l) = 0.055$) – see Table 3. Hence, $G(l) = G(a)$ only for $c = 1/1.26 = c_{\text{ASTM}}$. For a general c , the true difference is $\Delta G = G(a) - G_{\text{ASTM}}(l) = 3.3219 \log(1.26c)$, hence ΔG is positive for all $c > 1/1.26$ and negative in the opposite case. The absolute differences $\Delta G = 3.3219 \log(1.26c)$ are not large in specimens M, V, namely $-0.38 < \Delta G < 0.20$, consequently, the relative bias is very small. Only in some specimens of the type S, ΔG exceeds 1. It may be concluded that in the majority of examined cases, the difference between the Heyn $G(l)$ and Jeffries $G(a)$ ASTM numbers is negligible. This conclusion remains valid even for separated components in duplex structures (see below), where $-1 < \Delta G < 0.9$ was found (Table 4).

Duplex grain structures. In the majority of specimens, a duplex profile structure was observed. The coarser fraction usually differs also in the profile shapes; its profiles were frequently elongated with wavy boundary paths. However, grains of individual fractions do not form clearly delineated regions in sections of specimens M and V, usually only an isolated large profile testifies a local grain growth in the former ones. In spite of it, an attempt was made to divide the profile areas tentatively into coarser (c) and finer (f) fractions and to estimate their characteristics including also the area fractions $A_A(c) = 1 - A_A(f)$ (determined by point count) and lineal fractions $L_L(c) = 1 - L_L(f)$; the both estimates have been very similar and only the values of $L_L(c)$ are given in Table 5.

Table 5. Duplex grain structures S

Spec.	$L_L(c)$	$G_c(a)$	c_c	CV_{ca}	CV_{cl}	$G_f(a)$	c_f	CV_{fa}	CV_{fl}
S7	≈ 0.4	≈ 0	≈ 0.55	–	–	7.0	0.90	1.20	0.60
S1	≈ 0.06	≈ 1.4	–	–	–	6.1	1.02	1.05	0.75
S4	0.69	1.63	0.42	0.74	0.58	6.71	1.05	1.24	0.67
S3	0.69	1.37	0.68	0.81	0.65	6.13	0.85	1.05	0.58
S6	0.65	1.37	0.63	1.05	0.55	5.18	0.65	0.90	0.55
S5	0.67	1.22	0.89	0.93	0.53	6.01	1.25	1.13	0.65
mean)*	0.62	1.1	0.63	0.88	0.57	6.19	0.95	1.10	0.6

)* Specimens S1, S7 not included in the coarse fraction means

Table 6. Estimates of the volume intensity N_V

Spec.	Source	Ew	\bar{c}	c'	c''	\bar{N}_A [mm ⁻²]	$[\bar{N}_V]_{\bar{N}_A}$ [mm ⁻³]	\bar{N}_L [mm ⁻¹]	$[\bar{N}_V]_{\bar{N}_L}$ [mm ⁻³]	CV_v
M	<i>w-s</i>	1.16	0.81	0.8	0.583	3212	145 600	61.7	136 900	1.0
	ASTM	1.16	0.794	0.8	0.566		145 600		133 000	
S)*	<i>w-s</i>	1.24	1.25	0.724	1.01	282	3 429	14.68	3195	≈ 4
	ASTM						3 788		1791	
Sc	<i>w-s</i>	1.5	0.66	0.54	0.29	17.8	40	5.36	45	0.8
	ASTM						40		87	
Sf	<i>w-s</i>	1.2	0.95	0.76	0.70	668	13 120	26.0	12 300	1.1
	ASTM						13 812		9 948	
V	<i>w-s</i>	1.16	0.78	0.8	0.55	54.8	325	7.99	281	1.0
	ASTM						325		289	

)* Specimen S7 not included

Unfortunately, for specimens of the type M and V, the values of CV_{ca} for the coarser fractions have been usually smaller than the minimum possible values of $CV_a = 0.53$ (the value corresponding to the isohedral tiling by tetrakaidecahedrons). Consequently, the division was incorrect because small profiles of coarser grains were not properly recognized and specimens of these types were considered as monodispersed. On the other hand, continuous regions of small profiles could have been observed in the specimens of the type S and, consequently, the separation of two grain fractions was possible and successful (Table 5). Only one coarse profile was observed in specimen S1 and two coarse profiles in specimen S7; the extremely coarse profile of S7 was incomplete – see Fig. 4. Consequently, the coarse fractions of these two specimens were not included in the detailed analysis (Tables 5, 6).

4. Discussion

Planar analysis. It follows from Table 3 that the factor c differs substantially from the value postulated by ASTM Standards only in heterogenous grain structures S. Otherwise, the ASTM approach and the interchangeability of Heyn and Jeffries procedure can be safely accepted. This conclusion is rather general; the acceptable bounds of c are $\frac{2}{3} < c < \frac{5}{3}$, hence $-0.3 < \Delta G < 1.1$ for a wide range of tessellations.

The difficulties encountered in separating two components constituting the sections of specimens M, V can also be expected in general unless the profile fractions are identifiable otherwise than by the profile size only. Values of $CV a < 0.53$ or of $CV l < 0.471$ are reliable proofs of an unsuccessful separation.

The fraction separation in sections of specimens S demonstrates the overall inhomogeneous grain growth during the thermal treatment at $T \geq 980^\circ\text{C}$: the finer fraction is slightly coarser than profiles of specimens M and the coarser fraction is comparable with profiles of specimens V. Moreover, a local exaggerated growth producing profiles of extreme size is documented.

There is no systematic effect of time and temperature on the specimens of the type M and (with the exception of the specimen M4), the differences between the specimens are not substantial. Hence, only the mean values of all characteristics for specimens M are given in what follows. Averaged are also the characteristics of the specimens V even when their scatter is considerable. Such average values of G , ΔG and c have been calculated from the average values of N_A , N_L , whereas coefficients of variations of individual specimens were averaged directly (Table 5).

3D analysis. The second aim of the present paper is to comment on the possibilities of estimating also the volume intensity N_V of grains. The proposed approach is based on the estimate of the factor c and coefficients of variance $CV a$, $CV l$. A useful tool for the analysis of tessellations is the w - s diagram [1] (a substantial part of it is described in detail also in [3, 4]). In this diagram (Fig. 6), each *unit* tessellation is represented by a point $[\mathbf{E}w, \mathbf{E}s]$ in the rectangular coordinate system. Miscellaneous tessellations depending on some parameter t like cell shape, type of clustering of the tessellation generating process etc. are plotted as parametric curves $C(t) = \{\mathbf{E}w(t), \mathbf{E}s(t) | t \in [t_1, t_2]\}$. For example, the thick dash-dotted curve is the well-known Johnson-Mehl model with a variable nucleation rate, the thick full curve describes Voronoi tessellations generated by Neyman-Scott Poisson globular cluster field. The mean number of clustered points as well as the nucleation rate increase when moving down to the left lower corner of the diagram. The detailed description of the diagram, in particular the definitions of the particular curves, is in papers [1, 3, 4]. Here an overall character of the diagram is considered, namely the possible relation between point locations and the values of the coefficients of variation $CV a$ and $CV l$ – Figs. 6 and 7, respectively. The location of a

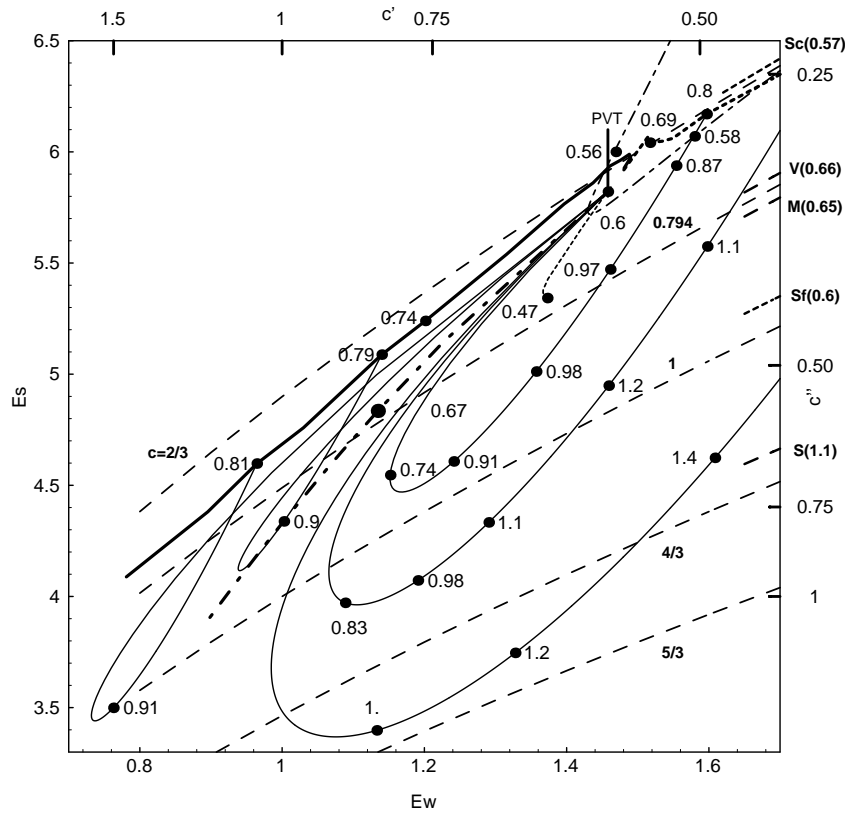


Fig. 7. The w - s diagram of the selected unit tessellations and the values of the coefficient of variation CVl . The constant value curves of the factor c are shown for selected values $2/3$, $c_{ASTM} = 1/1.26 \approx 0.794$, 1 , $4/3$, $5/3$ (dashed). Only short segments of the curves $c = \text{const.}$ for the observed values of \bar{c} are shown near the frame with the specimen notation and the values of CVl in parentheses.

general tendency is sufficiently perceptible. The point denoted by 0.56 describes the tiling by rhombic dodecahedra (generated by a face-centred cubic lattice). Its neighbourhood is filled up by other tessellations with equiaxial cells of mild or no size dispersion like the tiling by regular tetrakaidecahedra (generated by a body-centred cubic lattice and achieving the smallest possible value of $CVa = 0.53$), by the Poisson-Voronoi tessellation (generated by the stationary Poisson point process and denoted PVT; the point $CVa \approx 0.7$), and by tessellations generated by displaced lattices (e.g. the dotted curve joining the point labelled by 0.56 with the PVT point 0.7, corresponds to a displaced fcc lattice). The coefficients of variation increase when moving from this area of their low values in all directions. Down along the diagonal there are located already mentioned Johnson-Mehl and

clustered globular tessellations, the wedge-shaped area between them is filled up by self-intersecting loops of tessellations with an extreme size dispersion of predominantly equiaxial cells (they are generated by Bernoulli globular cluster fields [1]). The mean cell volume ratio of three populations composing the tessellations described by the loop with the level of 1.9 at its tip is $1 : \approx 70 : \approx 10^{-6}$. The profiles induced by the cells of the finest fraction are nearly completely missing in sections and in order to account for them, the factors c', c'' must be large.

The point with $CV a = 1.0$ (at the JM curve) lies in the central part of the diagram, and its values of c', c'' are very close to the recommended ASTM values as noted by Horálek [14]. Even this tessellation has a considerable size dispersion, and, consequently, the values of N_V are systematically overestimated when the recommended ASTM values are used to estimate the grain intensity of more regular structures of the Poisson-Voronoi or displaced tiling types.

The tessellations lying near the right upper corner of the diagram and farther in this direction are formed by non-equiaxial cells. The V-shaped dash-dotted curve describes tilings by hexagonal prisms with a variable c/a ratio (the upper and lower branches characterize rods and plates, resp.) and extends to infinity with $c/a \rightarrow 0, \infty$. Also the monodispersed wedge-like tessellations generated by Poisson spherical cluster fields (for details see [1, 13]) are located similarly as the hexagonal plates (along a nearly parallel thick dashed curve). Such non-equiaxial monodispersed cells are hit by section planes and lines with a comparable probability, and, consequently, the values of c', c'' factors are rather low and approach zero if $c/a \rightarrow \infty$ as well as if $c/a \rightarrow 0$. The increase in $CV a$ values is less pronounced here than when moving along the diagonal in the reverse direction because the profile size dispersion is mainly due to the sectioning variability.

Finally, the coefficients of variation also increase when moving to the right lower corner or horizontally to the right. Tessellation located here are mixtures of large equiaxial cell and numerous non-equiaxial and perhaps also partly oriented cells (they are generated by Bernoulli spherical cluster fields). With respect to their shapes and orientation, they may be hit by section planes but missed by section lines and the other way round, consequently, there are no systematic changes in the values of c', c'' .

The values of the coefficient of variation $CV l$ are presented in an equivalent $w-s$ diagram (Fig. 7). However, the differences in the values across the diagram are rather small and demonstrate the loss of information caused by low-dimensional probes. A reliable estimation of $CV l$ must be based on a very numerous chord population.

By inspection of the $w-s$ diagram, also the differences in the values of the factor c can be understood; selected curves of a constant value of c are shown in Fig. 7. Recalling its definition and the planar Crofton relation $\mathbf{E}a = \mathbf{E}l\mathbf{E}p/\pi$, the formula $c = \pi^2\mathbf{E}a/(\mathbf{E}p)^2$ must hold (p is the profile perimeter). Consequently, c is small for

sections of non-equiaxial tessellations like are the tilings by hexagonal prisms and other similar tessellations. The ASTM value $c = 1/1.26$ nearly equals the $\pi^2 a/p^2$ value of an arbitrary circle, namely $\pi/4 = 1/1.273$, and it is then nearly correct for sphere-like tetrakaidecahedral tiling as well as for other tessellations with equiaxial cells, even when their size dispersion is high. On the other hand, it is too small for mixtures of large equiaxial cells with small flat and rod-like cells.

Estimates of the spatial grain intensity N_V according to the ASTM recommendation are summarized in Table 6 (ASTM lines). The values $\bar{c}, \bar{N}_A, \bar{N}_V$ are the mean values with respect to all examined specimens of given type, consequently $\bar{c} = \overline{N_A/N_L^2} \neq \bar{N}_A/\bar{N}_L^2 = \bar{c}$ as N_A, N_L are not independent. For example, $\bar{c}_M = 0.843$, $\bar{c}_V = 0.858$. As the values of \bar{c}, \bar{c} for specimens M, V are close to the assumed ASTM value $c = 0.794$, the ASTM estimates $[\bar{N}_V]_{\bar{N}_A}, [\bar{N}_V]_{\bar{N}_L}$ do not differ substantially. However, the situation is different in the case of specimens S. High values of \bar{c}, \bar{c} in the cases S, Sf give $[\bar{N}_V]_{\bar{N}_A}$ considerably greater than $[\bar{N}_V]_{\bar{N}_L}$ and small \bar{c}, \bar{c} of the Sc fraction gives much smaller $[\bar{N}_V]_{\bar{N}_A}$ than $[\bar{N}_V]_{\bar{N}_L}$. w - s diagram can be helpful in such cases.

Thin dashed curves in Fig. 6 and denoted by X(Y) at their intersections with the frame are the curves $c = \text{const.}$ with $\text{const.} = \bar{c}_\bullet$ estimated for specimens M, V, S and the fractions Sc, Sf with the corresponding values of CV $\bullet a$ in the parentheses. Then, the position of the examined tessellation in the w - s diagram must be tentatively found such that the values of CV a and CV l are plausible. The corresponding coordinate $\mathbf{E}w$ is then specified, together with the value of c used to estimate the factors c', c'' , and, finally, the estimates $[\bar{N}_V]_{N_A}, [\bar{N}_V]_{N_L}$ are calculated (for details see [3, 4]).

For specimens M and V, $\bar{c} \approx c_{\text{ASTM}} = 0.794$, hence the ASTM value $\mathbf{E}w = 1.16$ with CV $a = 1$, CV $l = 0.67$ seems to be suitable. Then $c' = 0.8$ and the ASTM estimate of $[\bar{N}_V]_{\bar{N}_A}$ is accepted. In order to estimate $[\bar{N}_V]_{\bar{N}_L}$, the slightly corrected value of $c'' = c' c^{3/2}$ is used. The both estimators then give rather similar values.

In the case of specimens S, the ASTM estimates of N_V differ considerably because of the difference between the observed value of \bar{c} and the recommended value 0.794. Moreover, the observed values of the coefficients of variations CV a , CV l are much higher than those expected for the Johnson-Mehl point CV $a = 1$ underlying the ASTM approach. The point of intersection of the segment joining labels 2.2 and 3.5 in Fig. 6 (labels 0.98 and 1.2 in Fig. 7) with the curve $c = 1.25$ seems to be a plausible location for specimens S. Similarly, the values $\mathbf{E}w = 1.5$ and 1.2 are proposed for Sc, Sf, respectively, even when the both observed coefficients of variations are somewhat smaller than those in such locations in the diagrams. All the results are summarized in Table 6; note the much better agreement in the values of $[\bar{N}_V]_{\bar{N}_A}, [\bar{N}_V]_{\bar{N}_L}$ estimated on the basis of w - s diagram.

Finally, in the last column of Table 6, the estimates of the spatial coefficient of variation are given. For smaller values of CV a , CV l , they can be obtained from the

empirical equations given in [3]. The range of their validity is met by specimens Sc, Sf and slightly exceeded by specimens M, V. The values of CV v given in Table 6 have been obtained from the CV a values; CV l values give estimates typically lower by 30–40%. For specimens S with the values far outside the range of validity of the formulae, the theoretical w - s diagram with labeled model values of CV v instead of CV a , CV l has been used.

5. Summary

The presented results demonstrate the possibilities of the approach based on stochastic simulations of the model grain structures. It is shown that the w - s diagram serves as a helpful tool for spatial grain size estimation in certain cases and offers an illustrative explanation of possible deviations between grain size estimates based on profile and intercept count. The attempts to separate the components of heterogeneous grain structures are of particular importance. On the basis of estimated fraction values of variation coefficients CV a , CV l , completely unsuccessful separations can be excluded.

Acknowledgements

This research was supported by the Slovak Agency for Science VEGA, contracts No. 2/6097/99, No. 2/1009/21, and by the Grant Agency of the Czech Republic (contract No. 201/99/0269 – I.S.).

REFERENCES

- [1] SAXL, I.—PONÍŽIL, P.: Materials Characterization, 46, 2001, p. 113.
- [2] <http://fyzika.ft.utb.cz/voronoi/>
- [3] SAXL, I.—SÜLLEIOVÁ, K.—PONÍŽIL, P.: Kovove Mater., 39, 2001, p. 396.
- [4] VELGOSOVÁ, O.—SAXL, I.—BESTERCI, M.: In: Proc. 3rd International Conference on Materials Structure & Micromechanics of Fracture. Ed.: Šandera, P. Vutium, Brno, Brno University of Technology 2001, CD ROM p. 223–231.
- [5] SAXL, I.—PONÍŽIL, P.: Appl. Math., 47, 2002, 157.
- [6] GLADMAN, T.—PICKERING, F. B.: JISI, 202, 1967, p. 653.
- [7] ŠEVČÍK, A.: Trans. of The University of Košice, 3, 1999, p. 9.
- [8] ŠEVČÍK, A.—KOHÚTEK, I.: Trans. of The University of Košice, 4, 2000, p. 52.
- [9] ŠEVČÍK, A.—ČUPITA, F.—RUDNAYOVÁ, E.: Metallurgija, 33, 1994, p. 33.
- [10] ŠEVČÍK, A.: Mechanical properties of carbon steels with prevailing perlite structure. [In Czech]. Thesis, Mining Faculty, TU Košice 1999.
- [11] VANDER VOORT, G. F.: In: Practical Applications of Quantitative Metallography. ASTM STP 839, Philadelphia, ASTM 1982, p. 85.
- [12] SAXL, I.—PONÍŽIL, P.: In: STERMAT'2000, Proc. Sixth Int. Conf. Stereology and Image Analysis in Materials Science. Eds.: Wojnar, L., Rozniatowski, K. Cracow, Polish Society for Stereology 2000, p. 373, p. 379.
- [13] HORÁLEK, V.: Materials Characterization, 25, 1990, p. 263.
- [14] SAXL, I.—PONÍŽIL, P.: Acta Stereologica, 17, 1998, p. 237, p. 247.

Received: 9.7.2001